Modeling the nonlinear cortical response in EEG evoked by wrist joint manipulation

Vlaar, Martijn; Birpoutsoukis, Georgios; Lataire, John; Schouten, Alfred; Schoukens, Johan; van der Helm, Frans

DOI
10.1109/TNSRE.2017.2751650

Publication date
2018

Document Version
Final published version

Published in
IEEE Transactions on Neural Systems and Rehabilitation Engineering

Citation (APA)
Vlaar, M., Birpoutsoukis, G., Lataire, J., Schouten, A., Schoukens, J., & van der Helm, F. (2018). Modeling the nonlinear cortical response in EEG evoked by wrist joint manipulation. *IEEE Transactions on Neural Systems and Rehabilitation Engineering*, *26*(1), 205-215. https://doi.org/10.1109/TNSRE.2017.2751650

Modeling the Nonlinear Cortical Response in EEG Evoked by Wrist Joint Manipulation

Martijn P. Vlaar, Georgios Birpoutsoukis, *Member, IEEE*, John Lataire, *Member, IEEE*, Maarten Schoukens, *Member, IEEE*, Alfred C. Schouten, Johan Schoukens, *Fellow, IEEE*, and Frans C. T. van der Helm

***Abstract*— Joint manipulation elicits a response from the sensors in the periphery which, via the spinal cord, arrives in the cortex. The average evoked cortical response recorded using electroencephalography was shown to be highly nonlinear; a linear model can only explain 10% of the variance of the evoked response, and over 80% of the response is generated by nonlinear behavior. The goal of this paper is to obtain a nonparametric nonlinear dynamic model, which can consistently explain the recorded cortical response requiring little a priori assumptions about model structure. Wrist joint manipulation was applied in ten healthy participants during which their cortical activity was recorded and modeled using a truncated Volterra series. The obtained models could explain 46% of the variance of the evoked cortical response, thereby demonstrating the relevance of nonlinear modeling. The high similarity of the obtained models across participants indicates that the models reveal common characteristics of the underlying system. The models show predominantly high-pass behavior, which suggests that velocity-related information originating from the muscle spindles governs the cortical response. In conclusion, the nonlinear modeling approach using a truncated Volterra series with regularization, provides a quantitative way of investigating the sensorimotor system, offering insight into the underlying physiology.**

***Index Terms*— Electroencephalography, nonlinear system identification, regularization, robotic manipulator, Volterra series estimation.**

Manuscript received February 17, 2017; revised August 18, 2017; accepted September 8, 2017. Date of publication September 13, 2017; date of current version January 8, 2018. This work was supported in part by the European Research Council under the European Union's Seventh Framework Programme (FP/2007-2013) ERC Grant Agreement n. 291339, project 4DEEG: A new tool to investigate the spatial and temporal activity patterns in the brain, by ERC Grant Agreement n. 320378, project SNLSID: Data Driven Structured Modelling of Nonlinear Dynamic Systems, and by the Belgian Federal Government (Interuniversity Attraction Poles programme, IAP VII/19 - DYSCO). *(Corresponding author: Martijn P. Vlaar.)*

M. P. Vlaar is with the BioMechanical Engineering Department, Faculty of Mechanical, Maritime and Materials Engineering, Delft University of Technology, 2628CD Delft, The Netherlands (e-mail: m.p.vlaar@tudelft.nl).

G. Birpoutsoukis, J. Lataire, M. Schoukens, and J. Schoukens are with the ELEC Department, Vrije Universiteit Brussel, 1050 Brussels, Belgium.

A. C. Schouten is with the BioMechanical Engineering Department, Faculty of Mechanical, Maritime and Materials Engineering, Delft University of Technology, 2628CD Delft, The Netherlands, also with the Department of Physical Therapy and Human Movement Sciences, Feinberg School of Medicine, Northwestern University, Chicago, IL 60611 USA, and also with the Laboratory of BioMechanical Engineering, MIRA Institute for Biomedical Technology and Technical Medicine, University of Twente, 7500 EA Enschede, The Netherlands.

F. C. T. van der Helm is with the BioMechanical Engineering Department, Faculty of Mechanical, Maritime and Materials Engineering, Delft University of Technology, 2628CD Delft, The Netherlands, and also with the Department of Physical Therapy and Human Movement Sciences, Feinberg School of Medicine, Northwestern University, Chicago, IL 60611 USA

Digital Object Identifier 10.1109/TNSRE.2017.2751650

I. Introduction

HEALTHY movement control requires proprioceptive information from the periphery to reach the cortex; this sensory information is required for generating internal models enabling accurate planned movements (feedforward control) and for generating appropriate responses to disturbances (feedback control). Understanding the relationship between a movement and the cortical response improves the understanding of the sensorimotor system and can aid in unravelling sensorimotor dysfunction in movement disorders. Studying the dynamic relations within the sensorimotor system requires applying a proprioceptive stimulus, a clear task instruction and a cortical measurement technique with high temporal resolution such as electroencephalography (EEG) or magnetencephalography. EEG is a noninvasive technique with mild experimental restrictions with respect to movement and is widely available. Applying a continuous proprioceptive stimulus by manipulation a joint (e.g. wrist or finger) allows for studying the system in steady-state, i.e. when it is continuously and consistently engaged in processing sensory signals.

Cortical responses to continuous proprioceptive stimulation in healthy individuals have been investigated during both active [1]–[3] and passive [2] conditions using EEG. These studies revealed that the system under study is highly nonlinear. Therefore, studies using linear analysis techniques [1], [2] provide limited information about the functioning of the sensorimotor system; a linear approach to model the relation between proprioceptive stimulus and evoked cortical response can only capture 10% of the relationship [2]. Nonlinear modeling of this relation has not been done before. Compared to linear system identification techniques, nonlinear system identification techniques are less well developed, often computationally demanding and generally require some a priori knowledge.

This study sets out to obtain a nonparametric nonlinear dynamic model which consistently (i.e. consistently over different input signals) describes the relation between wrist movement and the average evoked cortical response recorded using EEG. The system is modeled using a truncated Volterra series with regularization [4]. Such a model requires limited a priori knowledge about the system, while allowing for a quantitative description of the dynamics of the sensorimotor system. The obtained models demonstrate how frequencies in the proprioceptive perturbation signal affect the frequency content of the evoked cortical response. Additionally, the noise in the response is quantified and a distinction is made between linear, 2nd order, and higher order nonlinear contributions to the evoked cortical response.

The experimental setup, used perturbation signals and modeling approach are presented in the Methods section. The Results section provides the characteristics of the recorded cortical signals, the performance of the models and their dynamic behavior. The Discussion section interprets the models based on physiology and provides a reflection on the approach, including suggestions for future work.

II. Methods

A. Participants and Experimental Protocol

Ten healthy right-handed participants (age range 22-25 years; 5 men) participated in the study [2]. The study was approved by the local ethics committee and all participants gave written informed consent prior to participation. Data of these participants were collected in a previous study; a summary of the relevant aspects of the experimental protocol will be presented here, for a full description the reader is referred to [2]. Participants were seated with their right forearm fixated to an arm support and their hand strapped to the handle of a robotic manipulator (Wristalyzer by MOOG Inc, Nieuw-Vennep, The Netherlands). Participants were instructed to relax their wrist and not react to the continuous angular perturbation applied by the robotic manipulator.

The perturbation signals were random phase multisine signals (i.e. the sum of several sinusoids, each with a random phase). In multisine perturbation signals, there is full control over the frequency content, leading to several advantages over random signals when performing system identification [5]. These advantages include the ability to detect even and odd nonlinear behavior, which is facilitated by the use of multisine signals with only odd frequency lines excited [5]. The perturbations were multisine signals with a period of 1 s, resulting in a fundamental frequency of 1 Hz. Only selected odd harmonics of the fundamental frequency were excited, namely 1, 3, 5, 7, 9, 11, 13, 15, 19, and 23 Hz. Exciting the nonlinear system using different phase realizations of a multisine signal (i.e. same amplitude per frequency, yet other random phases) allows for using different data sets for estimation and validation when modeling. Seven different multisine realizations were generated which were alternatingly applied during 49 trials of 36 seconds. Six seconds were removed from each trial to reduce transient effects, resulting in a total of 1470 recorded periods, i.e. 210 periods available for each of the seven realizations.

The angular perturbations had a root-mean-square (RMS) of 0.02 rad (see left insert in Fig. 1) and were applied with the wrist in a relaxed angle (i.e. slight flexion). The signals were designed to have equal power on the first three excited frequencies and a decreasing power for the higher frequencies

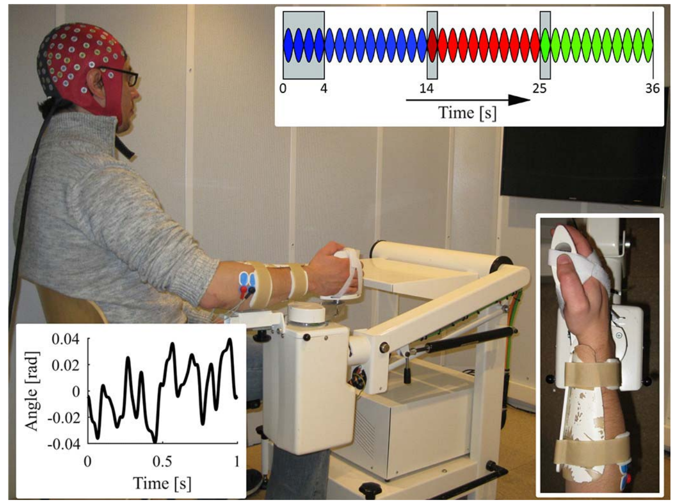

Fig. 1. Experimental setup. The right forearm of the subject is strapped into an armrest and the right hand is strapped to the handle, requiring no hand force to hold the handle. Participants were instructed to gaze at the screen, which showed a static target. The top-right insert shows a schematic representation of the composition of one 36s trial. Each lobe represents one 1s period of the perturbation signal and the three different colors represent different multisine realizations. Highlighted periods are excluded, leaving ten periods per realization in each trial for analysis. The bottom-left insert shows one of the realizations of the perturbation signal. The bottom-right insert shows a close up of the hand in the robotic manipulator. The wrist joint was aligned to the axis of rotation of the manipulator.

(−20dB/decade slope), which is a tradeoff between reduced predictability of the signal (to prevent anticipation) and capabilities of the robotic manipulator.

Cortical activity was sampled at 2048 Hz from 126 electrodes using an EEG amplifier (Refa by TMSi, Oldenzaal, The Netherlands). The handle angle of the robotic manipulator was, via a galvanic isolation transformer (TMSi, Oldenzaal, The Netherlands), recorded by the same amplifier.

B. Preprocessing

EEG data were high-pass filtered using a fourth order Butterworth filter with a cut-off frequency of 1Hz, which was applied in two directions to achieve zero-phase filtering. Independent component analysis (ICA) [6] was performed using the Infomax algorithm [7] as implemented in CUDAICA [8]. Subsequently, the data at component level were segmented into periods, resulting in $x^{[c,m,p]}(n)$, where x is the response, $c = 1, \ldots, C$ is the component ($C = 125$), $m = 1, \ldots, M$ is the multisine realization ($M = 7$), $p = 1, \ldots, P$ is the period ($P = 210$) and $n = 1, \ldots, N$ is the time index. An ideal filter was used to remove line noise (50 Hz) and to remove all frequencies from 100 Hz onward; i.e. signals were transformed to the frequency domain using the discrete Fourier transform (DFT) [9], all mentioned frequency lines were set to zero, and the signals were converted back to the time domain using the inverse DFT. Subsequently, all signals were resampled to 256 Hz ($N = 256$ samples).

To characterize the response of each component both the power in the average response (1) as well as the sample variance (2) were calculated at each frequency

$$\hat{E}_X^{[c,m]}(f) = \left| \frac{1}{P} \sum_{p=1}^{P} X^{[c,m,p]}(f) \right|^2 \quad (1)$$

$$\hat{\sigma}_X^{2[c,m]}(f) = \frac{1}{P(P-1)} \sum_{p=1}^{P} \left| X^{[c,m,p]}(f) - \frac{1}{P} \sum_{p=1}^{P} X^{[c,m,p]}(f) \right|^2 \quad (2)$$

where $X(f)$ is the DFT of $x(n)$.

To find the component which is most associated with the perturbation signals, the noise-to-signal ratio (NSR) was calculated; the component with the lowest NSR demonstrates the most consistent response. The NSR is defined as

$$NSR^{[c,m]} = \frac{\sum_{f \in F} \hat{\sigma}_X^{2[c,m]}(f)}{\sum_{f \in F} \hat{E}_X^{[c,m]}(f)}, \quad (3)$$

where F is the set of considered frequencies. For each participant, the NSR of each component c was determined by calculating the NSR over all frequencies and by subsequently averaging across realizations m. The signal of the component with the lowest NSR is defined as $y^{[m,p]}(n)$ and this signal was used for subsequent modeling. This signal was averaged over the recorded periods to reduce noise, and was subsequently defined as $y^{[m]}(n)$ and transformed to the frequency domain using the DFT, resulting in $Y^{[m]}(f)$. Similarly, the recorded input signal (i.e. wrist joint angle) was averaged over the recorded periods, giving $u^{[m]}(n)$ and transformed to the frequency domain, resulting in $U^{[m]}(f)$. The preprocessed data have been made available at http://ieeexplore.ieee.org.

C. Distinguishing the Spectral Contributions

The frequency content of the response of a static nonlinear system is governed by the order of the system as well as by the frequency content of the input signal. A quadratic static nonlinear system ($y = u^2$, which is an even nonlinearity) generates an output spectrum containing all possible combinations of two (positive or negative) input frequencies. In the case where only one input frequency is excited (e.g. f_0), the output will contain $f_0 + f_0 = 2f_0$, and also $f_0 - f_0 = 0$. This concept extends for higher order systems and is described in more detail in [10, p. 43, Fig. 9].

By the virtue of exciting only the odd frequency lines in the perturbation signals, the frequencies in the averaged output signal can be split into four groups. The first frequency group ($f_{\{1\}}$) consists of the excited frequencies in the input signal. The response at these frequencies will represent the linear contributions as well as part of the higher order odd (e.g. 3rd, 5th and 7th order) nonlinear contributions. The second group ($f_{\{2\}}$) consists of all the frequencies that can come from 2nd order nonlinear contributions ($f_{\{1\},1} \pm f_{\{1\},2}$), as well as part of the higher order even (e.g. 4th and 6th order) nonlinear contributions. The third group ($f_{\{3\}}$) consists of all odd frequencies not in $f_{\{1\}}$, which are the result of higher order odd (3rd order or higher) nonlinear contributions. The fourth and final group ($f_{\{4\}}$) consists of all even frequencies not in $f_{\{2\}}$, which are the result of higher order even (4th order or higher) nonlinear contributions. The total power in the signal can be split amongst these frequency groups to determine their individual contributions. Additionally, in all frequency groups there are still noise contributions present, given that the NSR is not reduced to zero. The NSR per frequency group is calculated using (3). The noise level in the averaged output signals puts a theoretical limit on the modeling accuracy, as that portion of the output data cannot be explained by a model.

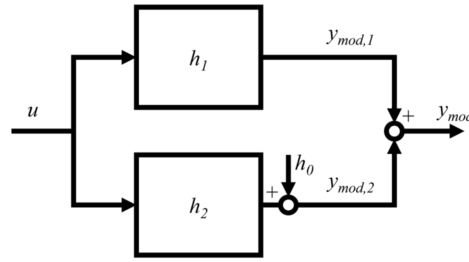

Fig. 2. Block schematic of the model structure. The top branch is a linear model which governs the output at the excited frequencies (i.e. $f_{\{1\}}$). This model is estimated by calculating the linear frequency response function. The bottom branch is a nonlinear model which is estimated using two terms of the Volterra series, namely the 2nd order kernel h_2 and the 0th order kernel h_0. The 2nd order kernel governs the output at $f_{\{2\}}$. The 0th order kernel is included to account for the potentially nonzero-mean signals generated by the 2nd order kernel.

D. Model Structure

The block scheme in Fig. 2 illustrates the modeling approach. The relation between joint angle (input) and cortical response as represented by the selected component (output) is modeled. The model consists of two parallel branches, specifically one 1st order and one 2nd order model. The latter also includes a 0th order model; due to filtering, the recorded output signal is zero-mean, yet the 2nd order model should not be restricted to produce a zero-mean output. The models in the two branches can be obtained in two separate modeling steps, as the 1st order model can only affect the output at $f_{\{1\}}$, and the 2nd order model can only affect the output at $f_{\{2\}}$ (i.e. using an odd perturbation signal, the two models are orthogonal). As a final step the two models are combined.

The 1st order (linear) model h_1 will be estimated in the frequency domain at the excited frequencies ($f_{\{1\}}$) in the input and at the same frequencies in the output, resulting in the best linear approximation (BLA) [5]. The frequency domain representation of this model is defined as $H_1(f)$.

The 2nd order (nonlinear) model is estimated using a truncated Volterra series expansion [11], which is similar to a Taylor series expansion, yet it includes dynamics. Regularization is used to incorporate prior information during the modeling procedure. Namely, by assuming that the model parameters are correlated and that the models decay to zero after a certain time, appropriate penalties can be imposed on the model estimation, which results in estimated models of

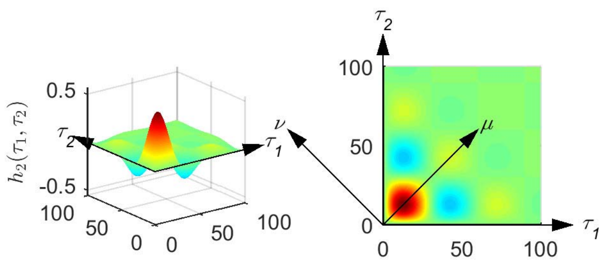

Fig. 3. Example of a function $h_2(\tau_1, \tau_2)$. The model corresponds to a Wiener-structure with a linear system followed by a square-operator. The left plot shows a 3D view of the model h_2. The right plot shows the same model from a top view, with additionally an indication of the directions μ and ν, along which the smoothness and decay rate of the model were quantified during regularization. The colors of the surface indicate amplitude.

substantially lower uncertainty. Regularization has previously been applied to linear [12], [13] and nonlinear [14], [15] model estimation, such that prior information about the estimated models is used during the identification step. Regularization imposing correlation and model decay for estimation of Volterra kernels has only recently been introduced [4].

E. Volterra Kernel Estimation Using Regularization

The true underlying even nonlinear contributions in the output y at $f_{\{2\}}$ (defined as y_2) are modeled with two terms of a discrete-time Volterra series [11], namely the 2$^{\text{nd}}$ order kernel h_2 and the 0$^{\text{th}}$ order kernel (i.e. constant term) h_0:

$$y_{mod,2}(n) = \sum_{\tau_1=0}^{d_2-1} \sum_{\tau_2=0}^{d_2-1} h_2(\tau_1, \tau_2)\, u(n-\tau_1)\, u(n-\tau_2) + h_0 \tag{4}$$

where $u(n)$ denotes the recorded joint angle, $y_{mod,2}(n)$ represents the modeled cortical response at $f_{\{2\}}$ (including 0 Hz), $h_2(\tau_1, \tau_2)$ is the 2$^{\text{nd}}$ order Volterra kernel, τ_1 and τ_2 denote lag variables, and d_2 corresponds to the memory of h_2. Without loss of generality, the estimated Volterra kernels are considered to be symmetric. An example of a function $h_2(\tau_1, \tau_2)$ is given in Fig. 3. Given the measured signals u and y, the goal is to efficiently estimate the Volterra kernel coefficients h_0 and $h_2(\tau_1, \tau_2)$. Equation (4) can be rewritten into a vectorial form as:

$$\bar{y}_{mod,2} = K \begin{bmatrix} h_0 \\ \theta_2 \end{bmatrix} \tag{5}$$

where $\theta_2 \in \mathbb{R}^{n\theta_2}$ is a vectorized version of h_2, $n\theta_2$ denotes the number of coefficients in h_2, $K \in \mathbb{R}^{(N\cdot M)\times\,(n\theta_2+1)}$ is the regressor matrix, and $\bar{y}_{mod,2} \in \mathbb{R}^{(N\cdot M)}$ contains the modeled output.

The regressor matrix K contains the input signal, which includes samples from time instants before the beginning of the input signal ($u(n)$, $n < 0$); however, due to the periodicity of the data the signal at those time instants is known.

The model parameters h_0 and θ_2 are estimated by minimizing the regularized least squares cost function:

$$\begin{aligned}\begin{bmatrix} \hat{h}_0 \\ \hat{\theta}_2 \end{bmatrix} &= \arg\min_{\theta} \left\| \bar{y}_2 - K \begin{bmatrix} h_0 \\ \theta_2 \end{bmatrix} \right\|^2 + \sigma^2 \begin{bmatrix} h_0 \\ \theta_2 \end{bmatrix}^{\mathrm{T}} \mathcal{P}^{-1} \begin{bmatrix} h_0 \\ \theta_2 \end{bmatrix} \\ &= \left(K^T K + \sigma^2 \mathcal{P}^{-1}\right)^{-1} K^T \bar{y}_2 \end{aligned} \tag{6}$$

where $\bar{y}_2$ is the vectorized recorded output data, which is assumed to be contaminated by zero mean i.i.d. white noise with finite variance σ^2. The first term of the summation in the cost function minimizes the difference between the recorded output and the modeled output in a least-squares sense. Matrix $\mathcal{P}$ penalizes the parameters such that prior information about the underlying dynamics of the true system is taken into account. The regularization matrix $\mathcal{P} \in \mathbb{R}^{(n\theta_2+1)\cdot(n\theta_2+1)}$ is constructed using a Bayesian perspective as explained in [12] and [15]. The matrix $\mathcal{P}$ is a block-diagonal covariance matrix:

$$\mathcal{P} = \begin{bmatrix} \mathcal{P}_0 & 0 \\ 0 & \mathcal{P}_2 \end{bmatrix}, \tag{7}$$

where $\mathcal{P}_0 = \mathrm{E}\left[h_0 h_0^{\mathrm{T}}\right]$, $\mathcal{P}_2 = \mathrm{E}\left[\theta_2 \theta_2^{\mathrm{T}}\right]$ and $\mathrm{E}[\cdot]$ denotes the mathematical expectation operator.

The prior information encoded in the matrix $\mathcal{P}$ assumes that the Volterra kernels used to describe the true system are decaying and smooth. The property of decaying refers to the fact that $h_2(\tau_1, \tau_2) \to 0$ for $\tau_1, \tau_2 \to \infty$. For the discrete-time Volterra series used in the current study, a smooth estimated kernel means that there exists a certain level of correlation between neighboring coefficients, which decreases the larger the distance between two Volterra coefficients. The properties of decaying and smoothness for the 2$^{\text{nd}}$ order Volterra kernel are encoded into the matrix $\mathcal{P}_2$. The (i, j)-element, which corresponds to $\mathrm{E}\left[\theta_{2,i}\theta_{2,j}\right] \forall i, j$ where $\theta_{2,i}\theta_{2,j}$ denote two Volterra coefficients in θ_2, is given by [4]:

$$\begin{aligned}\mathcal{P}_2(i, j) = c e^{-\alpha_\mu ||\mu_i|-|\mu_j||} e^{-\beta_\mu \frac{||\mu_i|+|\mu_j||}{2}} e^{-\alpha_\nu ||\nu_i|-|\nu_j||} \\ \times e^{-\beta_\nu \frac{||\nu_i|+|\nu_j||}{2}}\end{aligned} \tag{8}$$

where the coordinate system μ, ν is rotated 45 degrees counter-clockwise with respect to coordinate system τ_1, τ_2 (see Fig. 3):

$$\begin{bmatrix} \mu_i \\ \nu_i \end{bmatrix} = \begin{bmatrix} cos(45°) & -sin(45°) \\ sin(45°) & cos(45°) \end{bmatrix} \begin{bmatrix} \tau_{1,i} \\ \tau_{2,i} \end{bmatrix} \tag{9}$$

The so-called hyper-parameters α_μ and α_ν are used to control the smoothness property of the coefficients along the μ and ν direction, respectively. The hyper-parameters β_μ and β_ν determine the decay rate along the μ and ν direction, respectively. Hyper-parameter c is a scaling factor used to determine the optimal trade-off between the measured data and the prior information encoded in $\mathcal{P}_2$.

F. Efficient Tuning of the Prior Knowledge

All the hyper-parameters in (8), namely c, α_μ, β_μ, α_ν, β_ν, σ^2 and $\mathcal{P}_0$ are tuned using the input and output data by maximizing the marginal likelihood of the measured output [16]. Once the optimal values for these hyper-parameters are obtained, the model can be estimated from (6). Note that the memory length d_2 of the second order kernel is estimated separately (see Section II-I). Tuning the hyper-parameters in (8) is a non-convex optimization problem. To facilitate the algorithm and increase the probability of reaching the global maximum, the hyper-parameter space is restricted. Specifically: (i) $c, \sigma^2, \mathcal{P}_0 > 0$ because they are all directly linked to a measure of variance; (ii) The upper bound for α_μ and α_ν is 2 samples^{-1} which results in no correlation between the coefficients in the corresponding direction. The lower bound is set equal to $1/(5d_2)$ samples^{-1}, which would result in a strong correlation between all the coefficients of $h_2(\tau_1, \tau_2)$ and therefore an almost flat surface; and (iii) the upper bound for β_μ and β_ν is 2 samples^{-1}, which means that the estimated surface will decay in general almost immediately after one or two lags. The lower bound is set equal to $3/d_2$ samples^{-1}, which means that the estimated model will have virtually decayed to zero at the truncation lag of the model imposed by the memory d_2 [see (4)]. To further minimize the risk of resulting in a local maximum of the non-convex marginal likelihood function, the models presented in this paper have been obtained after multi-start optimization of the hyper-parameters.

G. Preparing the Data for Modeling

The perturbation signals were designed to have power at particular frequencies: the excited frequencies. Any power in the recorded wrist joint angle signal (i.e. the input to the human) at the unexcited frequencies was assumed to be due to nonlinear behavior of the robotic manipulator or noise; namely it is assumed that the human does not influence the angle of the robotic manipulator. The power at these frequencies was checked to be minimal and was subsequently removed from the recorded input signal to prevent the estimated model from using the power at the unexcited frequencies to explain the recorded output signals.

The recorded signals for the seven realizations were scaled to set their RMS to approximately one. The same scaling was applied to each realization to maintain their interrelations. The scaling was performed for both the input and output signals to prevent numerical problems in the nonlinear optimization of the hyper-parameters.

There is a time delay between the applied joint manipulation at the wrist and the evoked response in the cortex, which is a consequence of the limited conduction velocity in the afferent nerve fibers as well as of synapses in the pathway. For all participants the recorded output signals were shifted in time to impose a time delay of 20 ms.

H. Model Estimation Procedure

There are $M = 7$ multisine realizations available in the input and output data. Out of those seven, six realizations are used for estimation and the remaining realization is used for validation to assess the quality of the model. This procedure is repeated seven times to achieve seven-fold cross-validation, resulting in seven models for each branch in Fig. 2.

The linear and odd nonlinear contributions are modeled at the excited frequencies ($f_{\{1\}}$) in the input and output by calculating the average linear frequency response function for the different sets of estimation realizations:

$$\hat{H}_1^{[\upsilon]}\left(f_{\{1\}}\right) = \frac{1}{M-1}\sum_{w\in W_\upsilon}\frac{Y^{[w]}\left(f_{\{1\}}\right)}{U^{[w]}\left(f_{\{1\}}\right)}$$
$$W_\upsilon = \{w \in \mathbb{R} \mid 1 \le w \le M, w \ne \upsilon\}. \quad (10)$$

Here, $\hat{H}_1^{[\upsilon]}$ is the model obtained when using realization υ for validation, and U and Y are the frequency domain representation of the input (angle) and the output (selected independent component) respectively.

The even nonlinear contributions are also modeled using alternatingly six realizations for estimation and one for validation. The 0$^{\text{th}}$ and 2$^{\text{nd}}$ order kernels are estimated using (6), from $f_{\{1\}}$ in the input signal to $f_{\{2\}}$ in the output signal. As the required memory for the 2$^{\text{nd}}$ order kernel is unknown, different memory lengths in the range 10 to 75 samples (approximately 40 to 300 ms) are tried. This results in a set of models $\hat{h}_0^{[\upsilon,d_2]}$ and $\hat{h}_2^{[\upsilon,d_2]}(\tau_1, \tau_2)$, where υ is the realization used for validation and d_2 is the number of samples included as memory of the model [see Eq. (4)].

I. Selecting the Memory Length of the 2nd Order Kernel

Modeling the 1$^{\text{st}}$ order contributions (the BLA) generates one model for each validation realization and does not require further model selection.

For the 0$^{\text{th}}$ and 2$^{\text{nd}}$ order Volterra kernel, the modeling error on the validation datasets was calculated for all lags

$$\varepsilon^{[\upsilon,d_2]} = \sum_{n=1}^{N}\left(y_{mod,2}^{[\upsilon,d_2]}(n) - y^{[\upsilon]}(n)\right)^2, \quad (11)$$

where ε is the sum-squared error and $y_{mod,2}^{[\upsilon,d_2]}(n)$ is the modeled output using the corresponding 0$^{\text{th}}$ and 2$^{\text{nd}}$ order models (i.e. $\hat{h}_0^{[\upsilon,d_2]}$ and $\hat{h}_2^{[\upsilon,d_2]}(\tau_1, \tau_2)$), with validation dataset υ as input. The set of 0$^{\text{th}}$ and 2$^{\text{nd}}$ order models which demonstrated the lowest error were selected and were defined per validation realization υ as $\hat{h}_0^{[\upsilon]}$ and $\hat{h}_2^{[\upsilon]}(\tau_1, \tau_2)$. The obtained set of 2$^{\text{nd}}$ order models was transformed to the frequency domain using the two-dimensional DFT at a frequency resolution of 1 Hz, resulting in $\hat{H}_2^{[\upsilon]}(f_1, f_2)$.

J. Model Evaluation

The performance of the set of seven models for both the 1$^{\text{st}}$ and the 2$^{\text{nd}}$ order was evaluated by calculating the variance accounted for (VAF) on the validation data. As there are seven models available, the VAF is reported as its mean across the seven models including the standard deviation. The modeled output was calculated by summing the output of the 0$^{\text{th}}$, 1$^{\text{st}}$ and 2$^{\text{nd}}$ order models

$$y_{mod,val}^{[\upsilon]}(n) = \hat{h}_0^{[\upsilon]} + y_{mod,val,1}^{[\upsilon]}(n) + y_{mod,val,2}^{[\upsilon]}(n), \quad (12)$$

from which the mean was removed. The VAF can be calculated on the 1$^{\text{st}}$ and 2$^{\text{nd}}$ order contributions separately, or on the total modeled output using

$$VAF_{val}^{[\upsilon]} = \left(1 - \frac{var\left(y_{val}^{[\upsilon]}(n) - y_{mod,val}^{[\upsilon]}(n)\right)}{var\left(y_{val}^{[\upsilon]}(n)\right)}\right) \cdot 100\%. \quad (13)$$

For completeness, the VAF was also calculated on the data used for estimation. This was achieved by calculating the modeled output using the estimation data and concatenating the result into $y_{\text{mod},est,c}^{[\upsilon]}$. The six estimation realizations of

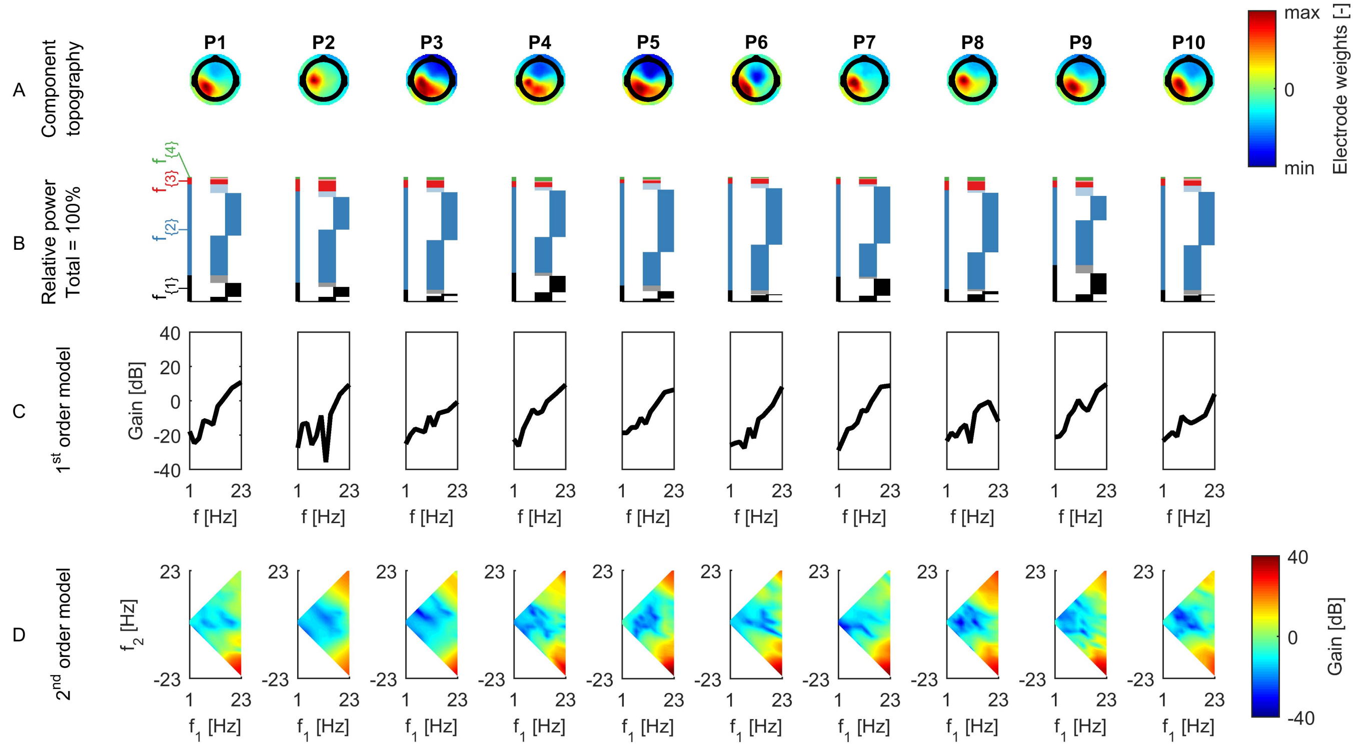

Fig. 4. Signal characteristics and models for each participant (represented by columns). Row A: Topographic representation of the weighing of electrodes in the independent component with the lowest NSR. Row B: Power distribution over four frequency groups in the output signal, indicated with four colors. The black and blue indented segment represent the VAF_{val} for the 1st and 2nd order models respectively. Shaded segments represent the noise level in that frequency group. See Fig. 5 for a detailed explanation for one representative participant. Row C: 1st order model for validation realization 5 (linear frequency axis). Row D: 2nd order model for validation realization 5 (linear frequency axis). See Fig. 6 for a detailed explanation for one representative participant.

the recorded averaged output signals $y^{[m]}$ were concatenated into $y^{[v]}_{est,c}$, enabling calculation of the VAF on the estimation data.

III. Results

A. Component Selection

Fig. 4A shows for each participant the topographic representation of the independent component (IC) with the lowest noise-to-signal ratio (NSR). These components for all participants suggest a similarly located cortical source in the contralateral sensorimotor cortices. For each participant, the signal of the shown component was used for modeling.

B. Signal Characteristics and Model Fit

Table I reveals that the noise level in the averaged recorded output signal is around 8% for all participants, indicating that the maximum achievable total VAF is around 92%. Additionally, Table I shows the ability of the models to fit both the validation and estimation.

Fig. 5 illustrates for one representative participant how each set of frequencies contributes to the averaged recorded output signal, and further splits the power into modeled (validation) data, unmodeled data and noise. Fig. 4B reveals that the bulk of the power in the averaged recorded output signal is concentrated in $f_{\{2\}}$ and that the contribution of $f_{\{3\}}$ and $f_{\{4\}}$ is small. This finding supports this paper's modeling approach, which focusses on the 1st (linear) and 2nd order (nonlinear) contributions in the recorded output signal.

Between the two models included, the main contribution in terms of VAF comes from the 2nd order model (around 39%). The model performance strongly depends on which realizations were used for estimation and which for validation. The VAF obtained from 1st order model (around 8%) is comparable to that obtained from modeling the electrode level response [2]. Besides the modeled data (46%) and the remaining noise in the averaged cortical signals (8%), there is still approximately 46% of unmodeled data.

TABLE I
Noise Levels and Model Fits

	NSR [%]	VAF_{val} total [%]	VAF_{val} H_2 [%]	VAF_{est} H_2 [%]	VAF_{val} H_1 [%]	VAF_{est} H_1 [%]
P1	15 (2)	45	34 (8)	42 (2)	11 (4)	14 (1)
P2	9 (4)	34	26 (12)	40 (12)	8 (3)	10 (1)
P3	7 (3)	40	38 (13)	48 (14)	2 (2)	4 (0)
P4	6 (1)	50	37 (8)	48 (9)	13 (5)	16 (1)
P5	11 (4)	56	50 (11)	58 (7)	6 (3)	8 (1)
P6	8 (2)	46	45 (25)	64 (3)	1 (2)	3 (0)
P7	4 (1)	60	46 (9)	52 (4)	14 (4)	15 (1)
P8	4 (1)	51	48 (7)	55 (7)	3 (4)	5 (1)
P9	15 (3)	36	19 (7)	34 (10)	17 (4)	20 (1)
P10	11 (3)	44	43 (21)	60 (6)	1 (1)	3 (0)
mean	*8 (5)*	*46 (8)*	*39 (10)*	*50 (9)*	*8 (6)*	*10 (6)*

The first ten rows represent the data for the ten participants. NSR presents the noise-to-signal ratio in the cortical response. VAF_{val} total presents the total variance-accounted-for on the validation data. The VAF is also reported separately for the 2nd and 1st order models (H_2 and H_1 respectively) on both the validation and estimation data (VAF_{val} and VAF_{est} respectively). Mean (and standard deviation in parenthesis) across different realizations are presented. The last row represents the mean (and standard deviation in parenthesis) of the results across all participants.

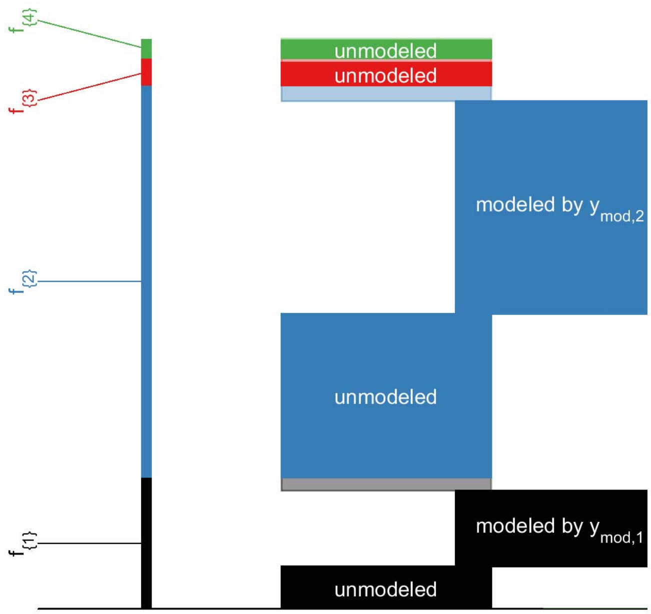

Fig. 5. Power distribution over frequency groups in the output signal for one representative participant (participant 4). Narrow bar on the left indicates the relative power in the four frequency groups. Wide bar segments on the right further split the power per frequency group into noise (shaded segments without text), unmodeled, and modeled data (the black and blue indented segment represent the VAF_{val} for the 1st and 2nd order model respectively). In this example, the total noise contributions are 6% and the total VAF on the validation data is 50%, where the 1st and 2nd order models explain 13% and 37% respectively (numbers from Table I). The power in $f_{\{3\}}$ and $f_{\{4\}}$ cannot be explained using the current model structure.

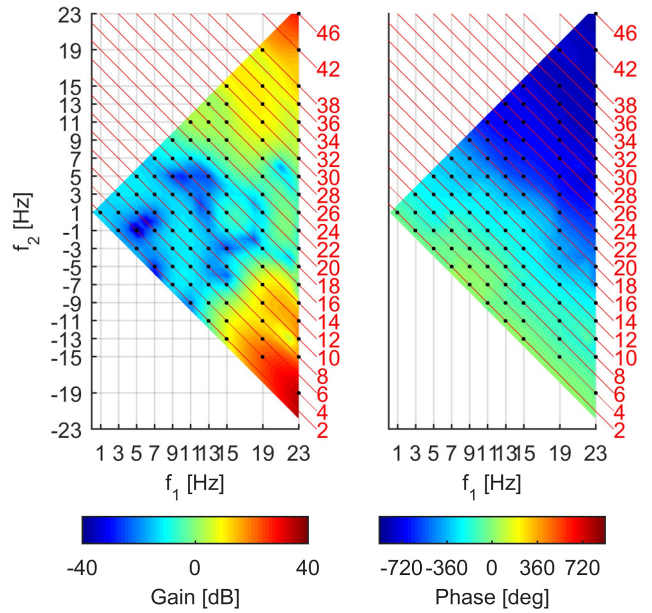

Fig. 6. Frequency domain representation of a 2nd order model (gain and phase) for one representative participant (participant 4) for validation realization 5. The obtained surface is symmetrical with respect to the line $f_1 = f_2$, as f_1 and f_2 are exchangeable in $\hat{H}_2(f_1, f_2)$. Additionally, as the model at the negative frequencies is the complex conjugate of the model at the same positive frequencies, the full behavior of the model can be represented using one quarter of the entire surface. Red lines and numbers at the right vertical axes indicate the frequencies (in Hz) in $f_{\{2\}}$ in the output signal that result from the excited input frequency combinations $f_{\{1\},1}$ (on the x-axes) and $f_{\{1\},2}$ (on the y-axis) that are indicated by the black dots. The gain plot on the left reveals that combinations of low input frequencies are strongly attenuated (i.e. gains are very low). The highest gains are found in the bottom right corner; in this region the model generates low-frequent output (as indicated by the red numbers) through the intermodulation of the high-frequencies in the input signal. Relatively high gains are also found in the top right corner; in this region the model generates high-frequent output through the intermodulation of again the high-frequencies in the input signal. This behavior can be classified as high-pass behavior.

C. Representative Models

Fig. 4C and Fig. 4D show for each participant one representative model for the 1st and 2nd order respectively (a detailed example of a 2nd order model is given in Fig. 6). Models obtained for the different validation realizations were very similar. The obtained 1st and 2nd order models for all validation realizations can be found online at http://ieeexplore.ieee.org.

The 1st order models shown in Fig. 4C on average only describe 8% of the output data, yet there exists a similarity for models obtained for the different participants; all 1st order models attenuate the low frequencies and amplify the high frequencies.

Fig. 6 shows the two-dimensional frequency response functions (gain and phase) of the obtained 2nd order model for one representative participant. Fig. 6 clearly illustrates which input frequencies contribute to the output. The model has the highest gain in the bottom-right corner, where high frequency input combinations generate low frequency output through intermodulation (e.g. $f_1 = 23$ Hz and $f_2 = -19$ Hz in the input signal contribute to $f_1 + f_2 = 4$ Hz in the output signal). The other region with high gains is found in the top right corner, which is again where the high frequencies interact. The lowest gains are found in the region where the low frequencies in the input interact. This same behavior can be observed in the models for all participants, as shown in Fig. 4D. Similarly to the 1st order model, the 2nd order models seem to exhibit high-pass behavior.

The memory of the selected 2nd order kernels [d_2 in (4)] strongly depended on which realization was used for validation and therefore varied within each participant (combined standard deviation of 15 samples). However, the average memory across realizations was similar across participants, with an average memory of 33 samples (standard deviation of 4 samples), corresponding to approximately 130 ms at a sampling rate of 256 Hz.

For each participant, the seven different models obtained from cross-validation were very similar. This holds for both the 1st order and the 2nd order models. Interestingly, the models obtained from the different participants are also similar; all obtained models strongly attenuate the low-frequent input signal and amplify the high-frequent input, resulting in high-pass behavior. The difference between the 1st order and 2nd order model is that although the 2nd order model acts as a high-pass filter, most power in the output is generated at the low frequencies.

IV. Discussion

The goal of this study was to obtain a dynamic nonparametric nonlinear model that could explain the observed cortical response recorded using EEG and evoked by continuous wrist joint manipulation. The high similarity in the cortical response across participants, in terms of location, distribution of power over frequencies, and observed dynamics in both the 1st order (linear) and 2nd order (nonlinear) parts of the model, allow for confident interpretation of the results. On average, 46% of the variance of the evoked cortical response could be modeled by the proposed approach; additionally, a clear distinction was made between parts of the cortical signal which could and could not be modeled. Around 8% of the averaged cortical signals could be attributed to noise. The obtained models reveal attenuation of low frequencies and amplification of high frequencies; this behavior can be interpreted as high-pass filtering, probably linked to dominant contributions from velocity-related information via Ia afferents originating from the muscle spindles. This study provides first evidence that the nonlinear cortical response to a proprioceptive stimulus can be quantitatively modeled, as was demonstrated using a truncated Volterra series expansion.

A. Selection of Cortical Response

This study focusses on the response most associated with the perturbation signal (i.e. with the lowest NSR). The independent component with the lowest NSR reveals a source at a similar location for each participant, namely the contralateral sensorimotor cortices. This finding is in line with previous literature on somatosensory evoked responses evoked by tactile stimulation of the hand [17] and by wrist joint manipulation [1], and is also expected based on where afferent fibers carrying proprioceptive and tactile information reach the cortex [18]. Besides the similarity in location, these selected cortical responses shared more characteristics across participants. The power distribution over frequencies is very much alike, where most power is concentrated in $f_{\{2\}}$ (see Fig. 4B). Additionally, the dynamics for both the 1st and 2nd order model revealed a comparable high-pass behavior for all participants. These similarities point towards a generalizable cortical response to the applied joint manipulation.

Although the participants also have other components which show a response related to the perturbation signal, none of those were as strong as the one selected for modeling. The number of independent components which could be represented well by a dipolar cortical source (residual variance <20% as determined using a dipole fitting algorithm and a standard head model) and which had relatively small noise contributions (NSR <30%), was on average 2.3 (standard deviation of 1.3) components. The power in the excited frequencies ($f_{\{1\}}$) in these components was on average 25.4% (standard deviation of 12.6), indicating that a linear model (the BLA) would also have limited performance for the other components associated with the perturbation signal. Other brain regions which are known to be active during somatosensory stimulation under passive conditions include the posterior parietal cortex [19] and the secondary somatosensory cortices [20]. The anatomical pathway for both tactile and proprioceptive information is the dorsal column-medial lemniscus pathway. This pathway connects the sensors in the periphery to the contralateral primary somatosensory cortex with only two intermediate synapses, namely in the spinal cord and the thalamus. Responses in other cortical areas are likely to be relayed by the primary somatosensory cortex to the secondary somatosensory cortex and the posterior parietal cortex [18]. In those cortical regions the somatosensory signals are further processed and integrated with motor control. The proposed modeling approach could also be applied to other parts of the cortex that respond to an external somatosensory stimulus.

B. Physiological Origin of the Evoked Cortical Response

The imposed joint rotation is registered by the sensory organs in the periphery and is transported to the cortical regions, where the response is recorded using EEG. This study cannot differentiate to what extent the obtained models are governed by the dynamics of the sensors or by the dynamics in the pathways between sensors, spinal cord and brain regions.

The applied joint manipulation stimulated at least the muscle spindles, Golgi tendon organs (GTO), joint capsules, and tactile sensors (e.g. Meissner's corpuscles, Pacinian corpuscles and Merkel's discs). Applying anesthesia which blocks afferents from tactile sensors and joint capsules did not substantially alter the evoked cortical response to passive finger flexion [21], to passive wrist extension [22], or to passive plantar flexions of the ankle [23]. Additionally, GTO do not generate strong signals under passive conditions, as a slack muscle has lower stiffness than the fibrils of the tendon that activate the GTO. Therefore, it is argued that in this particular study under passive conditions theevoked cortical response is mainly generated by muscle spindles. Muscle spindles sense both length and changes in length (i.e. velocity information). There are two types of fibers originating from the muscle spindles Information is transmitted via Ia and II afferent fibers, which have a high and medium conduction velocity respectively. The II afferent fibers provide position information, while Ia afferent fibers provide either velocity or position information, where the former is dominant during movement. The observed high-pass behavior could originate from the velocity sensitivity of the Ia afferents.

The contribution of the afferent pathways in the observed dynamic behavior is less clear. Insight can be obtained by including a measurement point within those pathways, for example by measuring the output of the muscle spindles using microneurography [28].

A possible explanation for the even nonlinear relation between joint manipulation and cortical response is found in the signals generated by muscle spindles in antagonistic muscles (i.e. wrist flexor and extensor); muscle spindles register velocity mainly when the muscle is lengthened and less when shortened [24], which might be altered by fusimotor activity [25], [26]. This unidirectional sensitivity makes the muscle spindle behave like a half-wave rectifier for velocity input. In contrast to the stretch reflex, which will activate different muscles depending on stretch direction, the cortical response to either direction generates similar responses in the cortex [27], [28] of which the locations are probably too near to be distinguishable when using EEG; possibly, the half-wave rectifiers in antagonistic muscle pairs together behave as a full-wave rectifier. The resulting insensitivity to direction is a typical characteristic of even nonlinear behavior.

C. Relation to Previous Continuous Joint Manipulation Studies

Cortical responses evoked by continuous mechanical stimulation have been studied before (see [29] for an overview); however, most of those studies stimulate the tactile system using high frequent vibrations. The number of studies that apply continuous joint manipulation is limited. The studies that do so, investigate the relation between joint movement and evoked cortical response by perturbing with one specific periodic joint perturbation signal and quantify the relation between stimulus and cortical response using either linear coherence [1], [30] or higher order cross-spectral coherence [31]. Linear coherence in combination with periodic perturbation signals impedes the detection of nonlinear behavior [32] and the obtained coherence is a mix of linear and nonlinear contributions. In contrast, higher order cross-spectral coherence (e.g. bi-coherence) does allow for the detection of nonlinear interactions. Although coherence can detect the strength of the coupling between input and output signal at certain frequencies, it fails to inform on how much of the output signal reflects that specific coupling. For example, in the case of significant coherence it can be concluded there exists a consistent relation between a frequency (or combination of frequencies) in the input and a frequency in the output signal; however it is unclear to what extent the output signal at that frequency is governed by the input signal at the investigated frequency. In contrast, the current study provides an approach for quantifying the nonlinear interactions in the sensorimotor system through a nonlinear dynamic model, which creates insight into which input frequencies in the perturbation signal govern the observed cortical response.

The use of multiple different perturbation signals is essential when modeling a nonlinear system; as the superposition principle does not hold, the model obtained from one perturbation signal is not generalizable to other perturbation signals, even if they have similar characteristics (e.g. RMS and excited frequencies). In the current study, this can be illustrated by estimating the linear relation between the input and output signals for just one realization of the perturbation signal; the resulting frequency response function does not reveal the high-pass behavior observed when using multiple realizations for estimation, and the VAF on any other realization is very poor.

Regardless of which approach is used to investigate the nonlinear relation between joint movement and cortical response, when exciting the system with one specific perturbation signal it is difficult to investigate the characteristics of the underlying system; the cortical response could drastically change when a different perturbation signal is used. Evidently, the use of a repeatedly applied transient stimulus, which is the most common EEG recording paradigm when the investigating somatosensory system, suffers from the same weakness.

D. Reflection on the Experiment

To further improve the perturbation signals for use in nonlinear modeling there are several options. Firstly, by using a longer period more frequencies can be accommodated. This would allow for including lower frequencies and more intermediate frequencies, thus creating a richer perturbation signal. Secondly, more phase realizations could be used, as apparently the seventh (i.e. validation) realization is in many cases still very different from the six used for modeling. By exciting the system with more phase realizations, the nonlinearity of the system is explored in more detail, which allows for more accurate modeling. Lastly, recording more periods per realizations would further reduce the noise level, although the noise is currently not the main issue as the noise level is much lower than the level of unexplained variance (8% and 46% respectively, see Table I). As one might expect, any of these three improvements would be accompanied by increased recording time.

The current study investigates the relation between joint manipulation and cortical response under passive conditions, i.e. without voluntary muscle activation. Under both passive or active conditions, any cortical efferent motor drive is not likely to be periodic to the perturbation; feedforward control synchronized to the perturbation would require a predictable perturbation signal, and feedback control via the cortex would be ineffective due to the relative large time delay of a cortical reflex loop. Thus, the evoked cortical response recorded during the execution of a task as described in the current study would reflect mainly sensory information processing.

In this study the joint was studied in a specific ‘operating point’. This point constitutes, amongst other aspects, the angle in which the wrist is studied, the frequency content and amplitudes of the perturbation signal, task instruction, and the efferent motor drive. With a change in any of these parameters the operating point could change, possibly requiring a different model. The current study illustrates that by controlling the ‘operating point’, it is possible to obtain similar models across participants.

E. Reflection on Modeling Approach

In the current study, the system under study is described by a 1st and 2nd order model. The power in $f_{\{3\}}$ and $f_{\{4\}}$ is small (around 10%, see Fig. 4B), indicating that the cortical response has little power at frequencies which can only be generated by 3rd and higher order nonlinearities. However, from this observation it cannot be concluded that there are no nonlinearities in the system higher than the 2nd order; high frequencies generated by higher order nonlinearities could be attenuated by low-pass dynamics. Any attempt to model higher order odd nonlinear behavior would result in a maximal VAF increase of around 9%, which corresponds to the unmodeled signal in $f_{\{1\}}$ and $f_{\{3\}}$. It would be beneficial to include higher order even Volterra kernels (e.g. a 4th order model); if the system under study indeed includes a rectifier as proposed before, higher order even kernels would be needed to better approximate that behavior. However, the estimation of higher order Volterra kernels would increase the number of parameters to be estimated, and therefore might require an experiment with a richer perturbation signal (i.e. more excited frequencies and increased period length).

Signals recorded at the scalp were decomposed in independent components using ICA. There are signal separation techniques which possibly result in a lower NSR [e.g. 33], thus increasing the quality of the data used for modeling and the maximum attainable VAF. These techniques have been mainly developed for separating cortical responses evoked by transient stimulation; their effectiveness for responses evoked by continuous stimulation needs to be further investigated.

All analyses were performed on data which was averaged across periods. The responses in a single period could not be observed due to the high NSR. Through averaging the NSR is improved; however, differences between responses in different periods (i.e. time-varying behavior) can no longer be observed. The time-variance of the periodic response was shown to be small in a previous study using the same experimental setup [29]. It would be interesting to further quantify the contributions of time-variance to the NSR. This could be achieved by performing an experiment with a high number of consecutively recorded periods, allowing for increased frequency resolution.

For all participants a time delay of 20 ms was imposed in the model, which is based on findings in literature for transient wrist joint manipulation [22], [28] as well as for electrical stimulation at the median nerve [22]. Although the actual time delay is participant specific (e.g. depending on arm length), due to the small differences observed in literature, here the time delay was set to 20 ms for all participants in the study.

The best performing 2^{nd} order models had an average memory of about 130 ms; hence, the impulse response of such a model will, including the imposed time delay of 20 ms, have an approximate duration of 150 ms. Such a response duration is close to those obtained in the contralateral sensorimotor cortex by applying a brief transient stimulus [28], [34].

Nonparametric modeling of a nonlinear system using a Volterra series has the major advantage of requiring limited a priori information about the exact nature of the nonlinearity, making it a powerful tool for exploring the characteristics of the nonlinear system under study. Hammerstein or Wiener cascades (e.g. the combination of a static nonlinearity with linear dynamics) are also often used to model nonlinear (neuro-)physiological systems [35], for example to study the relation between electrical nerve stimulation and muscle force output [36] or to study muscle reflexes due to joint movement [37]. The number of parameters required to estimate Hammerstein or Wiener cascades is substantially lower than for Volterra series estimation, but require prior assumptions about the nonlinearity. The drawback of a high number of parameters required for Volterra series estimation is mitigated by the use of regularization. Especially in the case of noisy data, regularization can reduce the uncertainty of the obtained models substantially. Nonparametric modeling is a necessary step before obtaining a quantitative dynamic nonlinear parametric model, which would provide crucial insights in the cortical involvement in processing of sensory information and cortical involvement in for example reflex modulation.

V. Conclusions

- A nonparametric nonlinear modeling approach requiring little assumptions is able to capture 46% of the relation between joint manipulation and evoked cortical response.
- For each participant, the similarity among the models obtained when using different parts of the data for estimation provides confidence in the estimated models.
- The observed consistency of the obtained models across participants indicates that these models are able to capture the behavior of the sensorimotor system.
- Multisine perturbation signals with only odd frequency lines excited reveal dominant even nonlinear behavior in the cortical response evoked by joint manipulation. Additionally, the odd and even contributions can be modeled separately due to orthogonality of odd and even models when using such a perturbation signal.

References

[1] S. F. Campfens, A. C. Schouten, M. J. A. M. van Putten, and H. van der Kooij, "Quantifying connectivity via efferent and afferent pathways in motor control using coherence measures and joint position perturbations," *Experim. Brain Res.*, vol. 228, no. 2, pp. 141–153, 2013.

[2] M. P. Vlaar, T. Solis-Escalante, A. N. Vardy, F. C. T. van der Helm, and A. C. Schouten, "Quantifying nonlinear contributions to cortical responses evoked by continuous wrist manipulation," *IEEE Trans. Neural Syst. Rehabil. Eng.*, vol. 25, no. 5, pp. 481–491, May 2017.

[3] Y. Yang, T. Solis-Escalante, J. Yao, A. Daffertshofer, A. C. Schouten, and F. C. T. van der Helm, "A general approach for quantifying nonlinear connectivity in the nervous system based on phase coupling," *Int. J. Neural Syst.*, vol. 26, no. 1, p. 1550031, 2016.

[4] G. Birpoutsoukis, A. Marconato, J. Lataire, and J. Schoukens, "Regularized nonparametric Volterra kernel estimation," *Automatica*, vol. 82, pp. 324–327, Aug. 2017.

[5] R. Pintelon and J. Schoukens, *System Identification: A Frequency Domain Approach*. Hoboken, NJ, USA: Wiley, 2012.

[6] S. Makeig, A. J. Bell, T.-P. Jung, and T. J. Sejnowski, "Independent component analysis of electroencephalographic data," in *Proc. Adv. Neural Inf. Process. Syst.*, 1996, pp. 145–151.

[7] A. J. Bell and T. J. Sejnowski, "An information-maximization approach to blind separation and blind deconvolution," *Neural Comput.*, vol. 7, no. 6, pp. 1129–1159, 1995.

[8] F. Raimondo, J. E. Kamienkowski, M. Sigman, and D. F. Slezak, "CUDAICA: GPU optimization of infomax-ICA EEG analysis," *Comput. Intell. Neurosci.*, vol. 2012, Jan. 2012, Art. no. 2.

[9] W. L. Briggs and V. Henson, *The DFT: An Owner's Manual for the Discrete Fourier Transform*. Philadelphia, PA, USA: SIAM, 1995.

[10] J. Schoukens, M. Vaes, and R. Pintelon, "Linear system identification in a nonlinear setting: Nonparametric analysis of the nonlinear distortions and their impact on the best linear approximation," *IEEE Control Syst.*, vol. 36, no. 3, pp. 38–69, Jun. 2016.

[11] M. Schetzen, *The Volterra and Wiener Theories of Nonlinear Systems*. New York, NY, USA: Wiley, 1980.

[12] T. Chen, H. Ohlsson, and L. Ljung, "On the estimation of transfer functions, regularizations and Gaussian processes—Revisited," *Automatica*, vol. 48, no. 8, pp. 1525–1535, 2012.

[13] J. Lataire and T. Chen, "Transfer function and transient estimation by Gaussian process regression in the frequency domain," *Automatica*, vol. 72, pp. 217–229, Oct. 2016.

[14] R. S. Risuleo, G. Bottegal, and H. Hjalmarsson, "A kernel-based approach to Hammerstein system identification," *IFAC-PapersOnLine*, vol. 48, no. 28, pp. 1011–1016, 2015.

[15] G. Pillonetto, M. H. Quang, and A. Chiuso, "A new kernel-based approach for nonlinear system identification," *IEEE Trans. Autom. Control*, vol. 56, no. 12, pp. 2825–2840, Dec. 2011.

[16] C. E. Rasmussen and C. K. Williams, *Gaussian Processes for Machine Learning*, vol. 38. Cambridge, MA, USA: MIT Press, 2006, pp. 715–719.

[17] A. Z. Snyder, "Steady-state vibration evoked potentials: Description of technique and characterization of responses," *Electroencephalogr. Clin. Neurophysiol./Evoked Potentials Section*, vol. 84, no. 3, pp. 257–268, 1992.

[18] E. Kandel, J. Schwartz, and T. Jessell, *Principles of Neural Science*, 4th ed. New York, NY, USA: McGraw-Hill, 2000.

[19] N. Forss *et al.*, "Activation of the human posterior parietal cortex by median nerve stimulation," *Experim. Brain Res.*, vol. 99, no. 2, pp. 309–315, 1994.

[20] H. Onishi *et al.*, "Neuromagnetic activation of primary and secondary somatosensory cortex following tactile-on and tactile-off stimulation," *Clin. Neurophysiol.*, vol. 121, no. 4, pp. 588–593, 2010.

[21] T. Mima, K. Terada, M. Maekawa, T. Nagamine, A. Ikeda, and H. Shibasaki, "Somatosensory evoked potentials following proprioceptive stimulation of finger in man," *Experim. Brain Res.*, vol. 111, no. 2, pp. 233–245, 1996.

[22] G. Abbruzzese, A. Berardelli, J. C. Rothwell, B. L. Day, and C. D. Marsden, "Cerebral potentials and electromyographic responses evoked by stretch of wrist muscles in man," *Experim. Brain Res.*, vol. 58, no. 3, pp. 544–551, 1985.

[23] A. Starr, B. McKeon, N. Skuse, and D. Burke, "Cerebral potentials evoked by muscle stretch in man," *Brain, J. Neurol.*, vol. 104, pp. 149–166, Mar. 1981.

[24] P. B. C. Matthews, "Muscle spindles and their motor control," *Physiol. Rev.*, vol. 44, no. 2, pp. 219–288, Apr. 1964.

[25] K. Appenteng, A. Prochazka, U. Proske, and P. Wand, "Effect of fusimotor stimulation on Ia discharge during shortening of cat soleus muscle at different speeds," *J. Physiol.*, vol. 329, no. 1, pp. 509–526, 1982.

[26] M. P. Mileusnic, I. E. Brown, N. Lan, and G. E. Loeb, "Mathematical models of proprioceptors. I. Control and transduction in the muscle spindle," *J. Neurophysiol.*, vol. 96, no. 4, pp. 1772–1788, 2006.

[27] E. Seiss, C. W. Hesse, S. Drane, R. Oostenveld, A. M. Wing, and P. Praamstra, "Proprioception-related evoked potentials: Origin and sensitivity to movement parameters," *NeuroImage*, vol. 17, no. 1, pp. 461–468, 2002.

[28] S. F. Campfens, C. G. M. Meskers, A. C. Schouten, M. J. A. M. van Putten, and H. van der Kooij, "Stretch evoked potentials in healthy subjects and after stroke: A potential measure for proprioceptive sensorimotor function," *IEEE Trans. Neural Syst. Rehabil. Eng.*, vol. 23, no. 4, pp. 643–654, Jul. 2015.

[29] M. P. Vlaar, F. C. T. van der Helm, and A. C. Schouten, "Frequency domain characterization of the somatosensory steady state response in electroencephalography," presented at the 17th IFAC Symp. Syst. Identificat. (SYSID), Beijing, China, 2015.

[30] H. Piitulainen, M. Bourguignon, X. De Tiège, R. Hari, and V. Jousmäki, "Corticokinematic coherence during active and passive finger movements," *Neuroscience*, vol. 238, pp. 361–370, May 2013.

[31] Y. Yang, T. Solis-Escalante, F. C. T. van der Helm, and A. C. Schouten, "A generalized coherence framework for detecting and characterizing nonlinear interactions in the nervous system," *IEEE Trans. Biomed. Eng.*, vol. 63, no. 12, pp. 2629–2637, Dec. 2016.

[32] B. E. Maki, "Interpretation of the coherence function when using pseudorandom inputs to identify nonlinear systems," *IEEE Trans. Biomed. Eng.*, vol. BME-33, no. 8, pp. 775–779, Aug. 1986.

[33] A. de Cheveigné and J. Z. Simon, "Denoising based on spatial filtering," *J. Neurosci. Methods*, vol. 171, no. 2, pp. 331–339, 2008.

[34] H. Onishi *et al.*, "Neuromagnetic activation following active and passive finger movements," *Brain Behavior*, vol. 3, no. 2, pp. 178–192, 2013.

[35] D. T. Westwick and R. E. Kearney, "Identification of a Hammerstein model of the stretch reflex EMG using separable least squares," in *Proc. 22nd Annu. Int. Conf. IEEE Eng. Med. Biol. Soc.*, vol. 3. Jul. 2000, pp. 1901–1904.

[36] E.-W. Bai, Z. Cai, S. Dudley-Javorosk, and R. K. Shields, "Identification of a modified Wiener–Hammerstein system and its application in electrically stimulated paralyzed skeletal muscle modeling," *Automatica*, vol. 45, no. 3, pp. 736–743, 2009.

[37] M. Mirbagheri, H. Barbeau, and R. E. Kearney, "Intrinsic and reflex contributions to human ankle stiffness: Variation with activation level and position," *Experim. Brain Res.*, vol. 135, no. 4, pp. 423–436, 2000.